Semiconductor racetrack resonator coupled to an Sbent waveguide: Influence of the coupling coefficients on the unidirectional operation

Received: 18 August 2020 | Revised: 29 October 2020 | Accepted: 10 November 2020

IET Optoelectronics

DOI: 10.1049/ote2.12015

The Institution of Engineering and Technology WILEY

ORIGINAL RESEARCH PAPER

Semiconductor racetrack resonator coupled to an S-bent waveguide: Influence of the coupling coefficients on the unidirectional operation

Giuseppe Giannuzzi | **Paolo Bardella**

Department of Electronics and Telecommunications, Politecnico di Torino, Turin, Italy

Correspondence

Giuseppe Giannuzzi, Department of Electronics and Telecommunications, Politecnico di Torino, Corso Duca degli Abruzzi 24, Turin 10129, Italy.
Email: giuseppe.giannuzzi@poliba.it

Abstract

Semiconductor ring lasers have attracted remarkable interest as laser sources in photonic integrated circuits. They result in bidirectional laser owing to the rotation symmetry between the two counter-propagating modes of the ring cavity. This symmetry can be broken embedding an S-bend waveguide in the racetrack resonator, which generates an unbalanced loss mechanism and a non-reciprocal gain between clockwise and counter-clockwise direction beams. The propagating field along the resonator in the undesirable direction is evanescently coupled to the S element in correspondence of two coupling regions and converted into the preferred one. The authors examined how the field coupling coefficients of the couplers impact the resonator unidirectionality. In numerical simulations, the authors changed the coupler gap distance and the coupler length of the directional couplers to scan the full range of variability of the coefficients. The simulated performances of the resonator are discussed in terms of the extinction ratio between the clockwise and the counter-clockwise modes as well as the power truly circulated in the two directions of the resonator net of all losses. The finite-difference time-domain method within Synopsys RSoft© suite was used to simulate the evolution of the counter-propagating field along the racetrack.

1 | INTRODUCTION

Semiconductor ring lasers (SRLs) have gained great interest due to their numerous benefits ranging from excellent performances to ease of integration in photonic integrated circuits (PICs) [1].

The ring cavity of the SRLs, featured by a symmetric resonator, supports two counter-propagating beams, that is, one circulating in clockwise (CW) direction and the other in counter-clockwise (CCW). Therefore, if unbalanced loss mechanism or non-reciprocal gain is not intentionally placed depending on the direction of propagation, a strong mode competition between the two counter-propagating lasing modes was predicted and observed [1–6]. For example, the competition gives rise to kinks in the light versus current characteristic, or, in other words, a bistable behaviour with a directional switching between the two instable unidirectional laser modes [2, 7]. In addition, the two modes can couple each other due to scattering or defects along the cavity, returning frequency splitting and spectral complexity [8].

However, several application fields demand unidirectional SRL [8–12], which means a more longitudinal mode purity in the pre-established direction of propagation and a reduced sensitivity to the back-reflections. Notable examples include optoelectronic gyroscope which uses SRL as source and sensing element [9], high-speed modulation by exploiting unidirectional whistle-geometry SRL as injection-locked laser [10], tuneable orbital angular momenta (OAM) microring laser as light sources emitting helical beams [8, 11] and high-repetition rate optical pulses by self-pulsing in unidirectional ring lasers [13].

Nevertheless, spontaneous unidirectional lasing was reported in the literature just in few works, that is for triangular SRLs [14, 15] and for large SRLs [16]. Such behaviour could be due to some imperfections along the cavity as well as due to the sidewall roughness of the waveguides promoting one lasing

direction between CW and CCW which was unpredictable in advance.

In the last decades, unidirectional emission from a bidirectional disk or ring cavity laser, has been achieved by breaking off their natural symmetrical behaviour with some tricks.

Liang et al. [17] forced the unidirectionality of a triangular ring laser cavity by employing a tapered section in one of the straight waveguides, providing loss of imbalance between the two opposite lasing directions, and a similar approach was recently used by Lee et al. [18] in a square ring cavity.

Other groups achieved the unidirectional lasing by introducing a feedback mechanism from the cleaved end-facet mirror [5, 6, 19] outside the ring where the undesirable field was reflected back and re-coupled in the SRL into the preferred direction. A similar strategy was used in heterogeneous micro-disk laser [20, 21].Unidirectional operation in SRL was obtained incorporating asymmetric elements into the laser cavity. Osinski et al. [10] studied the unidirectionality for a whistle-geometry semiconductor ring laser (WRL [21]), where the asymmetry was provided by a single Y-splitter which linked the ring to a straight waveguide. Such a connection introduced asymmetric optical losses between the two counter-propagating modes in the ring with a large difference between the corresponding photon lifetimes.

Hohimer et al. [2, 23] introduced an active S-shaped waveguide linked with two Y-splitters to the semiconductor ring diode laser to redirect part of the CCW field into the opposite CW one. Cao et al. [24] applied the same S-waveguide for an SRL with quantum-dot active region.

In the literature, different designs were proposed for the splitter between the SLR and the S-waveguide with the goal to more effectively suppress the unwanted mode favouring the mode propagating in the preselected direction [25, 26].

Several works [8, 11, 27, 28] included the S-waveguide inside the SRL by exploiting the evanescent coupling rather than Y-splitters to allow the mode conversion from CCW to CW or vice versa, according to the S orientation. Despite this change, the introduction of the S involved different intrinsic losses between the two counter-propagating modes in the SRLs. Sacher et al. [27] demonstrated the unidirectional laser oscillation for an SRL with an internal amplifying S-waveguide with 72% cross-coupled power coefficient, resulting in an extinction ratio between CW and CCW fields up to 18.6 dB. Ren et al. [8] and Hayenga et al. [11] recently exploited a similar active design for parity-time symmetric microring lasers to foster the unidirectional light emission used to generate vector vortex beams orthogonally to the chip growth plane. They experimentally measured the extinction ratio for the SRL with and without the S-waveguide achieving 28 and 0.1 dB, respectively.

Most of the cited papers regarding the unidirectional operation of the SRL with the S-waveguide are limited to a single design with fixed coupler power coefficients for the couplers or fixed splitting percentage in case of Y-splitter. Moreover, not every work reported such details which should be optimized for a higher unidirectionality of the device.

It is worthwhile to highlight that the structure consisting of a microresonator with an embedded S-shaped element, also referred to as taiji resonator, beyond the employment in unidirectional SRLs; it has recently shown a promising use as a unidirectional reflector in an optical integrated circuit [29]. The authors reported that best configuration of the unidirectional reflector was achieved with a critical coupling regime between the directional couplers of their device.

Finally, it should be mentioned that several works report unidirectional semiconductor disk laser (SDL) [20, 21, 30, 31] heterogeneously integrated on Silicon on Insulator (SOI) platform is compatible with Si complementary metal-oxide-semiconductor (CMOS) fab [1]. These works focused on different main aspects ranging from efficient coupling (hence sufficient phase matching) between the fundamental mode in the disk cavity and the fundamental waveguide mode [20, 30] to the integration of a passive distributed Bragg reflector (DBR) achieving an extra unidirectional gain resulting in a highly unidirectional emission of the laser [21]. The authors focused on the asymmetric resonator composed by a racetrack and an S-waveguide which mutually evanescently coupled the field in correspondence of the two coupling regions. We have explored the influence of the field through- and cross-coupling coefficients of the couplers on the unidirectional operation of the resonator. For this purpose, we have numerically simulated the evolution of both CW and CCW pulses launched in the asymmetric resonator using the finite-difference time-domain (FDTD) method evaluating the extinction ratio between the two counter-propagating modes in the cavity.

2 | DESIGN OF THE SLR WITH AN S-WAVEGUIDE

An S-bent waveguide inside the racetrack resonator was used to break off the natural symmetrical behaviour of the SRLs (Figure 1a), allowing the mode conversion from CCW to CW for our schematic. We briefly describe as this behaviour takes place, just considering only the racetrack and the S-waveguide of Figure 1a under two counter-propagating modes, CW and CCW, launched from the same position A (Figure 1a). We describe the optical events that they encounter along with a whole racetrack revolution; for the sake of simplicity, only the propagation of the fundamental mode TE of the waveguide was assumed, without internal and bending losses. Let us consider the CW mode. Its associated field moves from A to the coupling region B_1 between the two waveguides, propagating for a quarter of circumference without changes. In B_1, the field partially evanescently couple with the S-waveguide, propagating towards C_1, that is, the tapered S-end. Such field is spread outside the waveguide (radiation loss). The remaining CW field in the racetrack goes towards B_2 where analogue optical event happens to the previous one, hence the coupling field in the blind branch of the S-waveguide is radiated by the reversed taper C_2. Finally, the softened field propagates along the racetrack completing the round, reaching the starting point A.

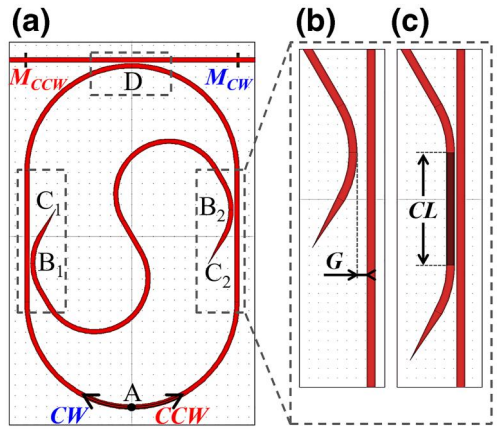

FIGURE 1 (a) Schematic of the racetrack resonator long 86.8 μm with the S-shaped waveguide which includes tapered terminators C_1 and C_2. CW and CCW represents the two counter-propagating modes, excited from the launch position A. The layout changes as a function of the coupler gap (G) distance and the coupler length (CL) of the directional couplers B_1 and B_2 as shown in (b) and (c), respectively

On the other hand, the CCW field launched from A when comes in B_2 is partially evanescently coupled with the S-waveguide and the rest transmitted ahead along the racetrack. The latter field undergoes the same splitting in correspondence of the subsequent coupler, B_1. As regard the CCW field coupled to the S-waveguide, it is driven within it reaching the coupler in the flip side of the S, that is, from B_2 to B_1 or vice versa. Due to the coupler, as always, the field is splitted between the two close waveguides; the part which returns into the racetrack is converted in the CW mode, while that transmitted towards the tapered end-S (C_2 or C_1) is loosed.

In summary, despite both CW and CCW fields intensity being reduced after a whole racetrack revolution, a part of the CCW mode is converted into the opposite one, thanks to the S-waveguide; therefore, the CW mode dominates the CCW mode.

Some important notes can be highlighted. First, the tapered ends-S are required to avoid the back reflection in correspondence of the extremities of the S-waveguide, which would result in the undesirable conversion from CW to CCW mode.

The power splitting in correspondence of the directional coupler depends on the value of the coupling coefficient, which in turn is controlled by the geometry of the coupling region. From one side, to reduce the CW round-trip losses, it would require that the coupled CW field with the S-waveguide is the smallest possible. From the other, to maximize the mode conversion from CCW to CW, it would be desirable to have a large coupling with the S-waveguide.

Our asymmetric resonator of Figure 1a was designed in order to study the influence of the field coupling κ and field transmission t coefficients of the directional couplers (between the racetrack and the S-waveguide) on the resonator unidirectionality. To vary in a wide range the coupling-transmission coefficients, the design of the Figure 1a changed the coupler gap (G) distance and the coupler length (CL) of the directional couplers B_1 and B_2, as shown in Figure 1b,c, respectively, preserving the original optical lengths of the racetrack.

The designed device was simulated with the FullWAVE module of the Synopsys© RSoft suite, based on FDTD method. As regard the waveguide geometry and the material, 0.45-μm-wide and 0.22-μm-deep silicon rib waveguide surrounded by silicon oxide as background material was used because it is able to support the propagation of the fundamental TE mode at 1.55 μm.

Indeed, the propagation of the electric field along such waveguide for the TE mode entails propagation loss and group velocity of 0.105 dB/cm and 0.275 c, respectively, where c is the speed of light in vacuum. [32].

Moreover, in order to reduce the computational cost of the simulations due to the 3D domain of the structure, the simulations were carried out using the effective refractive index method (2.5D). The simulation software included the spectral dispersion of optical properties.

The complex S-shaped waveguide design let to vary both its length and the CLs without changing the coupling regions B_1 and B_2. In this regard, the bending radius of the S-waveguide was fixed at 5 μm, corresponding to the minimum radius of the bent waveguide for which most Silicon Photonics platforms guarantees negligible curvature losses for the considered waveguide. This choice let us simulate a device of small dimensions that assures reduced simulation time cost. The device of Figure 1a consists of an 86.8-μm-long racetrack with an S-waveguide with half-length between the two directional couplers B_1 and B_2 and a straight waveguide placed at the top in Figure 1a which collects a part of the CW and CCW field circulating in the resonator for field measuring purposes. The directional coupler D evanescently couples the CW and CCW racetrack fields driving towards the two monitors, M_{CW} and M_{CCW}, located at opposite positions along the piking waveguide which are named as the circulating field emerging from the resonator that they track.

3 | RESULTS AND DISCUSSION

As already mentioned, we examined how the coupling coefficients of the directional couplers between the racetrack and the S-waveguide promoting the CW direction of propagation, hence, the device unidirectionality.

Figure 2 shows, in a 3D plot, the behaviour at 1.55 μm of κ^2 and t^2 coefficients for the directional couplers B_1 and B_2 as a function of the coupler gap distance and the CL. In detail, the coefficients are plotted for CL = 0 μm, when the coupler gap is reduced from 500 to 100 nm and for fixed G = 100 nm, when the CL is elongated from 0 to 6 μm. The coefficients come from simulations in RSoft of the directional coupler of Figure 1b,c and computed as the fraction of the power coupled P_{cross} from one waveguide to the other or the fraction of the power remaining $P_{through}$ in the original waveguide [33]:

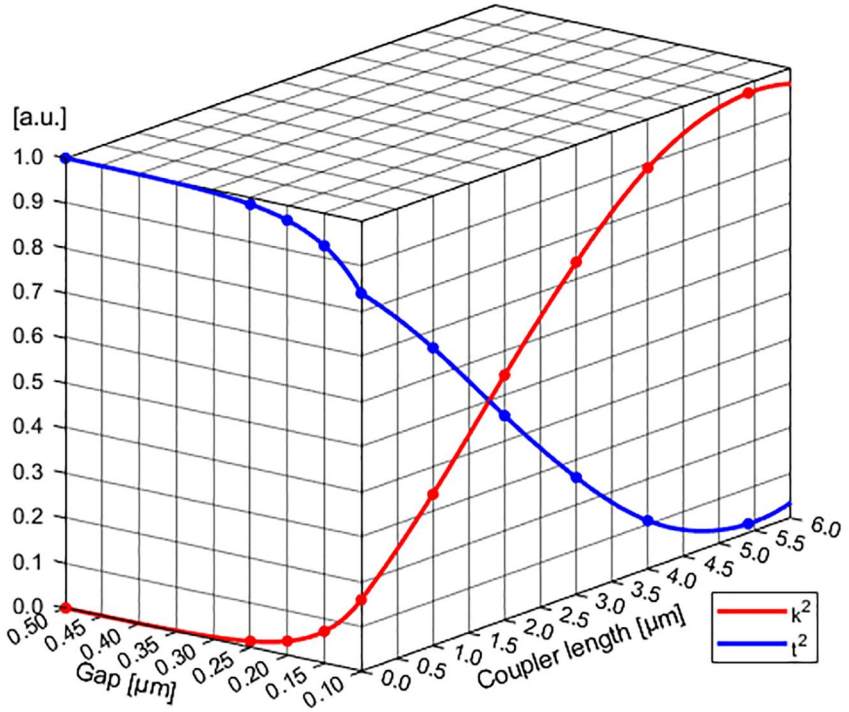

FIGURE 2 Field coupling (κ) and transmission (t) coefficients at $\lambda = 1.55$ μm as a function of the coupler gap distance and the coupler length of the directional couplers B_1 and B_2 as shown in Figure 1

$$\kappa^2 = \frac{P_{\text{cross}}}{P_0}\ ,\ t^2 = \frac{P_{\text{through}}}{P_0} \tag{1}$$

where P_0 is the input optical power.

The designed device of Figure 1a was simulated for a discrete number of coupling coefficients which are marked with filled dots in Figure 2, in way to cover the full range of variability, from 0 to 1. Such selected coefficients correspond to device configurations of appropriate G and CL values. Explicitly, from left to right, fixed CL = 0 μm and variable gap G = 0.5, 0.4, 0.3, 0.2, 0.1 μm and vice versa, fixed G = 0.1 μm and variable CL CL = 0, 1, 2, 3, 4, 5.4 μm. The last marked pair (κ; t) in Figure 2 was selected because the length LC = 5.4 μm corresponds to the cross-over length for the wavelength of 1.55 μm.

For simplicity's sake, we refer to the LC rather than LC + L_{bend} where the extra length takes into account the contribution to the coupling dues by the bent waveguides [33].

Concerning the directional coupler D between the racetrack and the piking waveguide, the gap distance is fixed to 100 nm for all the simulations, which corresponds to $\kappa = 0.6$ and $t = 0.8$ at 1.55 μm.

To investigate how the S-waveguide with different coupling coefficients impacts on the resonator unidirectionality, we excited inside the racetrack several optical pulses centred at 1.55 μm propagating in both the CW and CCW directions. This could be seen as spontaneous (or stimulated) emission of photons in the cavity. The use of the pulses as launch mode in RSoft let to take into accounts the dispersion behaviour of propagation at different wavelengths.

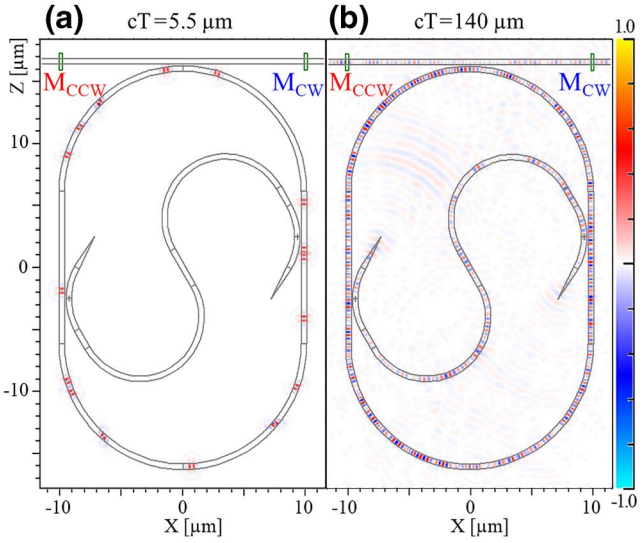

FIGURE 3 Contour Maps of the simulation for the device in Figure 1a with G = 0.1 μm and CL = 0 μm after (a) 5.5 μm and (b) 140 μm in unit of cT. The colours indicate the values of the field of the TE modes (CW and CCW)

The simulations were carried out exciting simultaneously 32 electromagnetic sources from 16 random positions along the racetrack which emit one pulse in the CW direction and the other in CCW one.

For example, Figure 3 shows two simulation frames of the device configuration with CL = 0 μm and G = 100 nm, for 16 launch positions randomly distributed along the racetrack. In detail, Figure 3a displays the TE mode field distribution after 5.5 μm in unit of cT with T time and c speed of light in vacuum

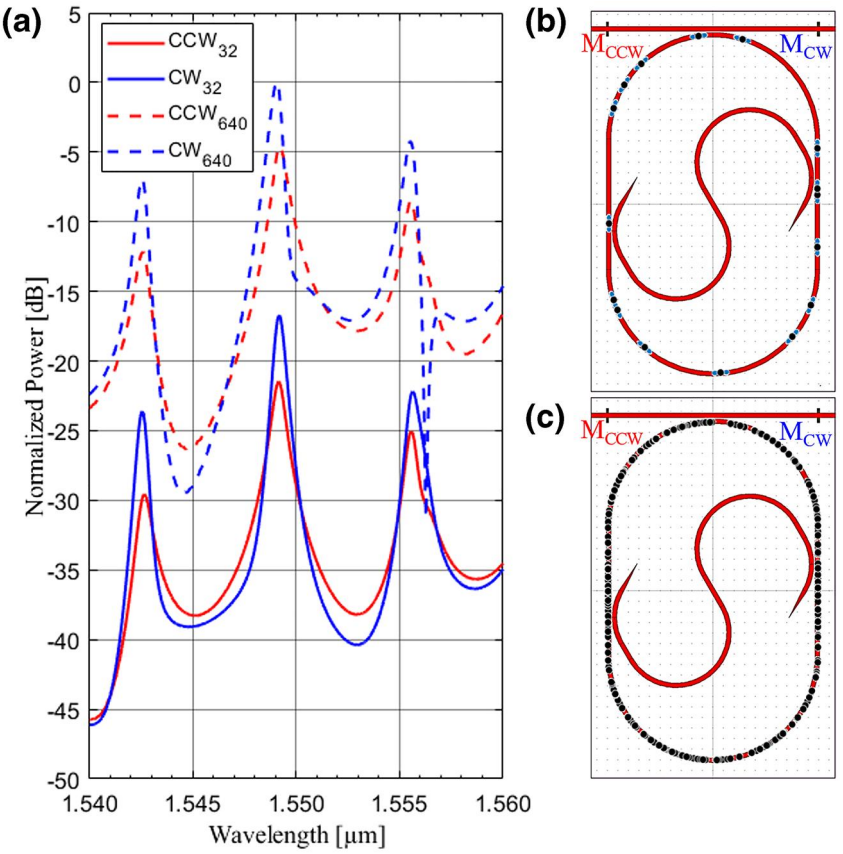

FIGURE 4 (a) Emission spectra relative to the simulations of the device of Figure 1a (G = 0.1 μm, CL = 0 μm) with launches distribution shown in (b) and (c), namely with 32 and 640 launches. The CCW and CW field are measured from the monitors M_{CCW} and M_{CW}, respectively

(i.e. 18.3 fs). Each pair of red spots represents the two counter-propagating pulses irradiated from the same launch position placed in the middle. Figure 3b shows the field distribution after 140 μm, highlighting the role of the S-waveguide in driving the CCW field evanescently coupled to the S-waveguide from one coupler toward the opposite one, reinforcing the CW one. From Figure 3b, it can be noted how part of the propagating fields in the device are collected by the piking waveguide propagating towards the two monitors mentioned earlier.

The final output optical spectra, evaluated at the monitors by the FDTD simulation for the case reported in Figure 3, are plotted in Figure 4a with solid lines for a wavelength interval of 20 nm centred around 1.55 μm. As expected in the case of the racetrack resonator, the spectra show peaks in correspondence of the resonant wavelengths but we focused on the resonance peak around 1.55 μm.

The different amplitudes between the CW and the CCW optical spectra highlight the asymmetric behaviour led by the S-waveguide on the two counter-propagating fields.

The same device configuration was simulated 20 times varying the distributions of the 32 random launches keeping fixed the monitors locations, untying the results from a peculiar launches distribution, and improving the accuracy of the results. In addition, a further analysis of the simulation results was conducted. The fields summation of the 20 simulations carried out for the same device configuration, return the overall field owed to the 640 launches. Figure 4a shows the overall wavelengths spectra (dashed lines) of the specific structure with CL = 0 μm and G = 100 nm, related to the 320 launches positions whose spatial distribution is depicted in Figure 4c.

Apart the peaks intensity between the resulting spectra from 32 or 640 launches shown in Figure 4a, the unbalance between the two counter-propagating modes CW and CCW was quantified in order to compare such results with that obtained by other device configurations. The unidirectionality of the device was expressed by the directional extinction ratio (DER) [8], expressed in decibel as follows:

$$\mathbf{DER} = \mathbf{10log_{10}}\frac{\mathbf{P_{CW}}}{\mathbf{P_{CCW}}} \tag{2}$$

that is the ratio in decibels of the power captured by the two monitors, P_{CW} by M_{CW} and P_{CCW} by M_{CCW}. The larger (positive) the DER value, the greater was the unidirectionality of the device (CW field dominant on CCW one).

From the simulations shown in Figure 4a, we obtained DER_{640} = 5.26 dB and DER_{32} = 4.78 dB, while the more representative DER value averaged on the 20 simulations is $\langle DER_{32} \rangle = (3.47 \pm 2.22)$ dB. Such values were calculated in correspondence to the resonant peak around 1.55 μm.

As already mentioned, 20 simulations with different launch positions were carried out for the coupling coefficients marked in Figure 2 or equivalently for the device configurations with

corresponding parameters G and CL. Figure 5 summarizes the comprehensive results of all simulations: for each device configuration was plotted the average and the standard deviation of the DER over 20 runs, $\langle DER_{32} \rangle$ with error bar, and the overall value DER_{640} (black stars). In addition, the grey bar represents the reference DER value obtained from the simulations of the lonely resonator without the S-waveguide. This is $\langle DER_{32} \rangle = 0.059$ dB $\pm$ 0.261 dB, which confirms no clear predominance between CW and CCW fields in case of symmetric resonator. Despite the expected DER value for a symmetric resonator was 0 dB, such non-zero value underlined the dependence of the measured field intensity from the positions of the launch sources and the monitors.

It is noticeable as the introduction of the S-waveguide moves the resonator response toward a unidirectional behaviour, especially reducing the gap distance and increasing the CL. For large gap, that is, 0.5 μm, or equivalently a coupling coefficient κ extremely low, the S-waveguide footprint looks negligible and not very useful for the unidirectional purpose. Reducing G until to 0.1 μm, passing from $\kappa \simeq 0$ to $\kappa = 0.4$, the unbalanced effect owed to the S-waveguide becomes noticeable; the CW field is more and more reinforced by the major fraction of CCW field coupled to the S-waveguide. We observe the most attractive results for the configurations with G = 0.1 μm and variable CL from 0 to 5.4 μm, due to the positive DER values, hence a CW mode predominant. Nevertheless, to a large variation of the coupling coefficients seen in Figure 2, from CL = 0 μm to the cross-over length, corresponds a gentle increasing of the average DER value. Similar comments for the analysis of the overall DER_{640} which values are consistent with the average DER previously discussed, depicting inside the error bar of $\langle DER_{32} \rangle$.

However, it is advisable to discuss how an increase in the value of CL, next to the gentle increasing of the DER, as discussed earlier, leads to an increasingly small power circulating in the resonator. Figure 6 shows the power of the resonant peak closest to 1.55 μm (normalized) versus the CL of the different device configurations simulated. The box plots for each CL depict the statistic distribution of the peak power values on the 20 simulations, both the CW and the CCW mode, which intensity strongly depends on the launch positions, as previously commented. The stars plot the overall CW and CCW fields on the 640 total launches. Each configuration highlights the predominance of the CW field (blue descriptors) with respect to the CCW one (red descriptors), hence the positive DER in Figure 5.

By comparing the powers for the different configurations, it emerges a decreasing trend by increasing the CL or equivalently rising the coupling between the racetrack and the S-waveguide. This power attenuation is ascribed to the field fraction coupled to the S-waveguide and spread outside the device by the S-terminators. We point out that such tapered terminators are essential to avoid the back reflections of the CW field into the unwanted CCW.

Consequently, a trade-off between the coupling coefficients and the attenuation power is required. In particular, the simulated configurations with G = 0.1 μm and CL ranged from 0 to 2 μm represent the better compromise solution to

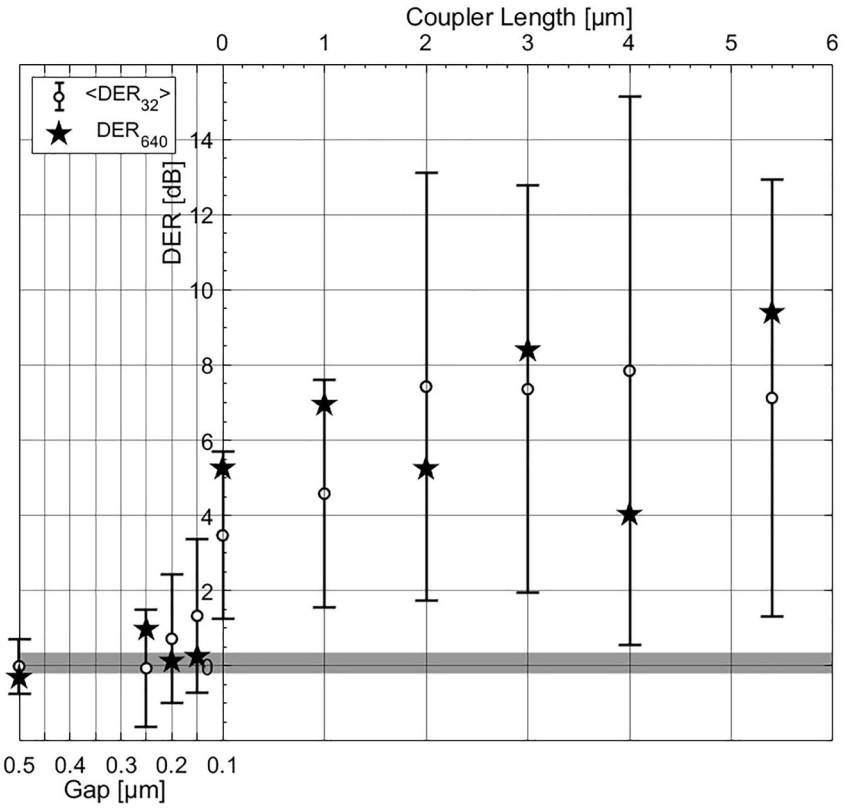

FIGURE 5 Directional extinction ratio (DER) versus the gap distance (bottom axis) and the coupler length (top axis) estimated to the peak resonator wavelength around 1.55 μm. The average DER and the standard deviation evaluated over 20 runs is plotted as blank dot with error bars while the overall DER on the 640 launches with filled stars. The horizontal grey bar represents the average DER value and std obtained without the S-shaped waveguide in Figure 1a, corresponding to the symmetric case

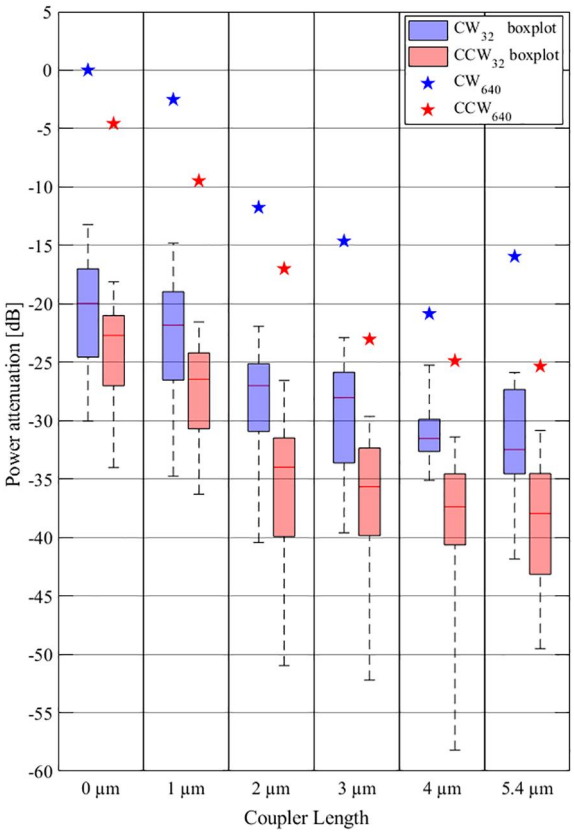

FIGURE 6 Power distribution for the resonant peak around 1.55 μm versus the coupler length (CL) for both CW and CCW propagating mode: the distribution on the 20 simulations for each CL was graphed as boxplot; the overall power by the 640 launches was plotted with stars

achieve positive DER, from 3 to 7 dB on average, saving power losses, namely κ from 0.40 to 0.74.

Our simulation results were obtained from merely statistical considerations on a discrete number of sources spread along the racetrack. Nevertheless, the DER positivity found in the configurations mentioned earlier, is expected to be enhanced operating with active resonator, as reported in the literature for SRL [1, 15]. Moreover, an active S-waveguide would encourage a stronger device unidirectionality, since the amplified radiation is then coupled back into the SRL in the preferred direction [23, 26].

4 | CONCLUSION

Many unidirectional SRLs have been proposed in the literature to improve the performances of the rotation symmetry ring lasers for suitable application fields.

The considered device consisted of a racetrack embedding an S-bend waveguide which drove the evanescently coupled field to the S-waveguide from CCW to CW propagation direction.

We studied the influence of the field coupling coefficients of the couplers on the unidirectionality of the resonator. Varying the design parameters of the couplers (gap distance and coupler length) we have explored the full range of variability of the coefficients from 0 to 1. Simulations were carried out by making use of the FullWAVE module of the Synopsys© RSoft suite, based on FDTD method. It is shown that varying the design parameters of the coupler enabled the unidirectional operation, namely modified the ratio between CW and CCW power while preserving the single mode light emission.

Our simulation results provide a careful reference in term of field coupling coefficients for future design of integrated unidirectional ring lasers: the range $0.40 \leq \kappa \leq 0.74$ results a good trade-off between the highest values of DER between CW and CCW modes and the power attenuation due to the overall losses of the resonator. Finally, the employment of an active biased S-waveguide could add a non-reciprocal gain in favour of the CW mode [24, 27] increasing the achieved DER values and will be the object of investigation of future works.

ACKNOWLEDGEMENTS

The authors would like to express their gratitude to Enrico Ghillino for motivating this work and the Synopsys support service, in particular Tung-Yu Su, for the helpful technical support.

ORCID

Giuseppe Giannuzzi https://orcid.org/0000-0002-1057-1873
Paolo Bardella https://orcid.org/0000-0003-1075-8264

REFERENCES

1. Mezosi, G., Sorel, M.: Semiconductor micro-ring lasers compact semiconductor. Lasers. 9783527410, 231–256 (2014)
2. Hohimer, J.P., Vawter, G.A., Craft, D.C.: Unidirectional operation in a semiconductor ring diode laser. Appl. Phys. Lett. 62(11), 1185–1187 (1993)
3. Sargent, M., III: Theory of a multimode quasiequilibrium semiconductor laser. Phys. Rev. A. 48(1), 717–726 (1993)
4. Yuan, G., et al.: Theoretical and experimental studies on bistability in semiconductor ring lasers with two optical injections. IEEE. J. Sel. Top. Quantum Electron. 14(3), 903–910 (2008)
5. Cai, X., et al.: Nonlinearity in semiconductor micro-ring lasers compact semiconductor. Lasers. 9783527410, 257–296 (2014)
6. Liang, D., et al.: Hybrid III-V-on-silicon microring lasers. MRS Proc. 1538, 363–369 (2013)
7. Mezösi, G., et al.: Unidirectional bistability in AlGaInAs microring and microdisk semiconductor lasers. IEEE Photonics Technol. Lett. 21(2), 88–90 (2009)
8. Ren, J., et al.: Unidirectional light generation in PT-symmetric microring lasers. 2018 Conf. Lasers Electro-Optics (CLEO) 26(21), 27153–27160 (2018)
9. Dell'Olio, F., et al.: Recent advances in miniaturized optical gyroscopes. J. Eur. Opt. Soc. 9(14013), 1–14 (2014)
10. Osinski, M., et al.: Structure-induced asymmetry between counter-propagating modes and the reciprocity principle in whistle-geometry ring lasers. Proc. of SPIE. 1034520, 70 (2017) https://doi.org/10.1117/12.2274604
11. Hayenga, W.E., et al.: Direct generation of tunable orbital angular momentum beams in microring lasers with broadband exceptional points. ACS Photonics. 6(8), 1895–1901 (2019)
12. Yu, C., et al.: Controllable optical bistability in double quantum dot molecule. IET Optoelectron. 12(4), 215–219 (2018)
13. Columbo, L.L., et al.: Self-pulsing in single section ring lasers based on quantum dot materials: theory and simulations. Opt. Express. 26(15), 19044 (2018)

14. Booth, M.F., Schremer, A., Ballantyne, J.M.: Spatial beam switching and bistability in a diode ring laser. Appl. Phys. Lett. 76(9), 1095–1097 (2000)
15. Ji, C., Booth, M.F., Ballantyne, J.M.: Low noise operation of a unidirectional triangular ring laser. Conference Proceedings – Lasers Electro-Optics Society Annual Meeting, pp. 945–946 (2005) https://doi.org/10.1109/LEOS.2005.1548323
16. Sorel, M., et al.: Unidirectional bistability in semiconductor waveguide ring lasers. Appl. Phys. Lett. 80(17), 3051–3053 (2002)
17. Liang, J.J., et al.: Unidirectional operation of waveguide diode ring lasers. Appl. Phys. Lett. 70(10), 1192–1194 (1997)
18. Lee, J.W., et al.: Selection of lasing direction in single mode semiconductor square ring cavities. J. Appl. Phys. 053101, 119(5), 1–7 (2016)
19. Oku, S., Okayasu, M., Ikeda, M.: Low-threshold CW operation of square-shaped semiconductor ring lasers (orbiter lasers). IEEE Photonics Technol. Lett. 3(7), 588–590 (1991)
20. Spuesens, T., et al.: Compact integration of optical sources and detectors on SOI for optical interconnects fabricated in a 200 mm CMOS pilot line. J. Light. Technol. 30(11), 1764–1770 (2012)
21. Mechet, P., et al.: Unidirectional III-V microdisk lasers heterogeneously integrated on SOI. Opt. Express. 21(16), 19339 (2013)
22. Smolyakov, G.A., Osi, M.: High-speed modulation analysis of strongly injection-locked semiconductor ring lasers. IEEE. J. Quantum Electron. 47(11), 1463–1471 (2011)
23. Hohimer, J.P., Vawter, G.A.: Unidirectional semiconductor ring lasers with racetrack cavities'. Appl. Phys. Lett. 63(18), 2457–2459 (1993)
24. Cao, H., et al.: Highly unidirectional InAsInGaAsGaAs quantum-dot ring lasers. Appl. Phys. Lett. 86(20), 1–3 (2005)
25. Withers, N.J., et al.: Highly unidirectional Y-junction S-section ring lasers. Phys. Simul. Optoelectron. Devices XVI. 6889, 688916 (2008)
26. Hyun, K.S., et al.: Selection of the lasing direction using S-bend in the semiconductor cavities. 2015 11th Conference of Lasers Electro-Optics Pacific Rim. CLEO-PR 2015. 3, 3–4 (2016) https://doi.org/10.1109/CLEOPR.2015.7376560
27. Sacher, W.D., et al.: Unidirectional hybrid silicon ring laser with an intracavity S-bend. Opt. Express. 23(20), 26369 (2015)
28. Giannuzzi, G., Ghillino, E., Bardella, P.: Geometry optimization of unidirectional integrated ring laser. In: SPIE OPTO (Ed.), SPIE Proceedings, pp. 112832H. (2020)
29. Calabrese, A., et al.: Unidirectional reflection from an integrated 'taiji' microresonator. Photonics Res. 8(8), 1333–1341 (2020)
30. Sinha, R., et al.: Tunable, room temperature CMOS-compatible THz emitters based on nonlinear mixing in microdisk resonators. J. Infrared, Millimeter, Terahertz Waves. 37(3), 230–242 (2016)
31. Kumar, R., et al.: An ultra-small, low-power all-optical flip-flop memory on a silicon chip. Opt InfoBase Conf. Pap., pp. 10–12.(2010)
32. Ahmadivand, A., Golmohammadi, S.: Comprehensive investigation of noble metal nanoparticles shape, size and material on the optical response of optimal plasmonic Y-splitter waveguides. Opt. Commun. 310, 1–11 (2014)
33. Chrostowski, L., Hochberg, M.: Silicon Photonics Design. Cambridge University Press (2015)

How to cite this article: Giannuzzi G, Bardella P. Semiconductor racetrack resonator coupled to an S-bent waveguide: Influence of the coupling coefficients on the unidirectional operation. *IET Optoelectron*. 2021;15:131–138. https://doi.org/10.1049/ote2.12015